symmetry

MDPI

Article

Application of the Finite Element Method for Analyzing the Vibration Characteristics of a Spindle System and Fault Diagnosis

Leilei Zhang [1,*] and Zisheng Wang [2]

[1] Department of Automation, Moutai Institute, Renhuai 564500, China
[2] School of Mechanical Science and Engineering, Huazhong University of Science and Technology, Wuhan 430074, China; zisheng8@mail.tsinghua.edu.cn
* Correspondence: zhangleilei@mtxy.edu.cn

Abstract: The performance of a spindle will gradually decline, the vibration intensity will increase, and the temperature rise will become abnormal with the accumulation of service time. Consequently, the accuracy of the machining product will not meet its production requirements. Studies on the variation characteristics of the spindle unit have clarified the reasons for its abnormal vibration and temperature rise, in principle, to help enterprises conduct preventive maintenance before any serious failure occurs and improve production efficiency. Based on the Timoshenko beam model and rotor dynamics theory, this study uses the finite element method (FEM) to analyze the vibration characteristics of the spindle rotor system. Moreover, it thoroughly analyzes the influence of the spindle bearing heat on the stiffness of the spindle system and identifies the resonance conditions of the spindle rotor within the power frequency range. This research has identified that when the vibration frequency of the spindle operates at a speed of 12,000 r/min, if its vibration frequency is lower than 200 Hz, it will be affected by abnormal vibrations during startup, which will weaken the health status of the spindle and reduce its service life. Similarly, when the working speed of the spindle is 30,000 r/min, if its vibration frequency is lower than 50 Hz, abnormal vibration will occur during startup and operation, thereby reducing its service life.

Keywords: vibration; spindle; fault diagnosis; predictive maintenance

check for updates

Citation: Zhang, L.; Wang, Z. Application of the Finite Element Method for Analyzing the Vibration Characteristics of a Spindle System and Fault Diagnosis. *Symmetry* **2024**, *16*, 1468. https://doi.org/10.3390/sym16111468

Academic Editor: Sorin Vlase

Received: 2 September 2024
Revised: 10 October 2024
Accepted: 22 October 2024
Published: 5 November 2024

Copyright: © 2024 by the authors. Licensee MDPI, Basel, Switzerland. This article is an open access article distributed under the terms and conditions of the Creative Commons Attribution (CC BY) license (https://creativecommons.org/licenses/by/4.0/).

1. Introduction

A spindle will experience varying degrees of thermal deformation in various parts under the combined influence of internal and external heat sources, an important factor affecting the machining performance of machine tools. For example, thermal prestress is generated inside the spindle rotor, accompanied by a certain degree of thermal bending, under the influence of a non-uniform thermal load, changing the frequency and eccentricity of the spindle rotation unit. The spindle will be subjected to a huge centrifugal force when it rotates at high speed, periodically impacting the spindle bearings, accelerating the bearing damage, and reducing the spindle's service time. Therefore, studying the thermal characteristics of the spindle in principle, finding measures to improve its thermal stability, transforming the thermal expansion of the bearing unit into a factor conducive to the bearing assembly, and analyzing its thermal vibration characteristics can improve the machining accuracy and work efficiency of computer numerically controlled (CNC) machine tools, provide diagnostic indicators for the health status of the spindle unit, and improve monitoring efficiency regarding the health status of CNC machine tools [1–8].

The study of thermal vibration characteristics of spindle components has long been a research focus. Wang et al. established a vibration model for a ceramic motorized spindle, with a focus on investigating the vibration behavior caused by interference (such as unbalanced forces) and thermal displacement. The results showed that thermal effects

and mechanical interference have a significant impact on the dynamic performance of the spindle and effective control methods to reduce vibration were proposed to improve the precision and stability of the ceramic motorized spindle [9]. Jin et al. conducted a comprehensive analysis using theoretical modeling, simulations, and experiments to study how these factors affect spindle performance [10]. Alfares et al. used analytical methods to investigate how temperature changes affect the mechanical behavior and performance of the system. The authors provided insights into thermal effects on bearing stiffness, load distribution, and overall spindle dynamics, contributing to a deeper understanding of how thermal factors can impact spindle-bearing system reliability and performance in practical applications [11]. Liu et al. developed a detailed analytical model that integrates thermal influences on system stiffness, vibrations, and load distribution. Through simulations and dynamic analysis, they explored how temperature changes affect the system's performance and stability. The findings provide valuable insights for improving spindle-bearing system design and operational efficiency by accounting for thermal variations [12]. Zhang et al. presented a detailed study on how a cooling system impacts the thermal performance of a spindle, aiming to improve heat dissipation and maintain optimal operating temperatures. Their research provides insights into the design considerations for effective cooling solutions for high-speed motorized spindles, helping to enhance spindle reliability and operational stability [13]. Dong et al. investigated how initial preload and spindle speed affect the thermal stiffness of machine tool spindle bearings. The study utilizes fiber Bragg grating (FBG) sensors to measure temperature and deformation, providing real-time data on thermal stiffness changes under different conditions. The findings highlight the significant impact of initial preload and rotational speed on bearing performance, offering valuable insights for optimizing thermal stiffness and improving the overall reliability of machine tool spindles [14]. Dinh et al. used analytical models to study the influence of temperature on spindle dynamics, bearing contact angles, stiffness, and overall system behavior. Their findings demonstrated how thermal variations can affect the spindle's operational accuracy and reliability, providing insights that contribute to optimizing spindle design for enhanced thermal management and performance [15]. Liu et al. analyzed the influence of various factors, such as spindle speed, tool geometry, and stiffness, on the dynamic performance of an assembly, which provided valuable insights into optimizing spindle–tool interactions for improving the precision and efficiency of optical grinding processes [16]. However, these models can only qualitatively analyze the dynamic response of the spindle-bearing system and it cannot be accurately simulated, since the previously mentioned spindle-bearing system models primarily combine nonlinear stiffness or quasi-static bearing models with rigid or finite-element spindle models. In summary, the dynamic characteristics of rolling bearings and the decreased mechanical equipment accuracy due to their heating up can seriously impact the stability and processing accuracy of mechanical equipment. Therefore, analyzing the basic dynamic characteristics of such elements using theoretical and experimental methods is crucial for identifying the primary influencing factors affecting the dynamic stability of shaft-type mechanical equipment to improve equipment stability and safety.

Cao et al. investigated the dynamic behavior of a turning electric spindle in a maglev with a variable mass system. They focused on the impact of changing mass distribution on the spindle's performance and stability. The results provide insights into optimizing spindle design for better performance in variable mass conditions [17]. Shi et al. presented a dynamic model of an aerostatic spindle that considered shaft deformation. They explored how shaft deformation influences spindle dynamics, leading to insights on improving spindle stability and precision in manufacturing processes [18]. Ye et al. investigated thermo-mechanical deformation in the ball screw system of a machine tool spindle feed system and provided a model for understanding how thermal effects interact with mechanical loads to affect system accuracy, with recommendations for improving spindle performance [19]. Cao et al. proposed a thermal error prediction model for CNC machine tool spindles based on linear correlation analysis, which helped improve the accuracy of

thermal error compensation, enhancing the precision of machining processes [20]. Guo et al. presented an enhanced algorithm to quickly identify thermal errors in machine tool spindles. The proposed method significantly reduces thermal equilibrium time, enabling more efficient machining operations by minimizing thermal distortions [21]. Lu et al. developed a digital twin-based model to predict thermal errors in CNC machine tool spindles. This approach improves real-time thermal error prediction, enhancing machining accuracy and reducing the errors caused by thermal deformation [22]. Miao et al. examined the dynamic behavior of a column-spindle system, taking into account the nonlinear characteristics of kinematic joints, and provided insights for optimizing machine tool dynamics [23]. Xu et al. investigated the influence of the pedestal and clearance fit on the dynamic behavior of spindle-bearing systems. Their study highlighted the effects of these factors on vibration and stability, thereby contributing to improvements in spindle-bearing design and performance [24]. Tian et al. analyzed the nonlinear vibration behavior of rolling bearings with a fractured flexible cage. The study revealed the impact of cage fractures on bearing dynamics, providing insights for detecting and mitigating potential faults in rolling bearings [25]. Hou et al. investigated the dynamic response of a dual-rotor system affected by non-concentricity due to inter-shaft bearing positioning deviations. Their study offers insights into the effects of such deviations on system performance, helping in the design and alignment of dual-rotor systems to improve operational stability [26]. Liu et al. explored how manufacturing errors influence the vibration characteristics of high-speed angular-contact ball bearings. The authors used dynamic analysis to identify the impact of these errors on bearing performance, thereby contributing to better quality control and precision in bearing manufacturing [27]. These papers provide a comprehensive overview of recent advances in spindle vibration analysis, with a focus on both theoretical modeling and practical monitoring techniques.

This study uses the finite element method (FEM) to analyze the vibration characteristics of the spindle rotor system. Moreover, it deeply analyzes the influence of the spindle bearing's heat on the stiffness of the spindle system and elucidates the resonance conditions of the spindle rotor within the power frequency range. Additionally, the general law for the variation of the low-order vibration frequency of the spindle-bearing system with the stiffness of the supporting bearing is given. This research proposes a new method for diagnosing spindle faults, which can help researchers to better understand the operating status of the spindle.

2. Spindle Structure

2.1. Spindle

The most commonly used spindles in the processing of 3C products (computers, communication, and consumer electronics) can be divided into two types: electric and mechanical spindles. The electric spindle has a built-in motor to reduce intermediate transmission links, and the mechanical spindle is connected using an external motor drive. This section focuses on the finite element modeling method for the spindle structure and bearing rotor system.

Both types of spindles have advantages and disadvantages. Electric spindles, which have high rotational speeds, are suitable for processing highly rigid materials but are difficult to maintain and have high usage costs. Mechanical spindles have simple structures and are easy to maintain, meeting the processing requirements of most mechanical products in use. Presently, both types of spindles are widely used, based on project experience. The general structure of a mechanical spindle is shown in Figure 1. As shown in Figure 2, mechanical spindles have two driving methods: a transmission belt connection and a direct motor connection (separate spindle), respectively. For small machining centers, the maximum working speed of the spindle when connected using the transmission belt is usually around 15,000 rpm, and the speed of the direct spindle can reach up to 25,000 rpm. The main limiting factor for the spindle speed is the DN value corresponding to the spindle bearing.

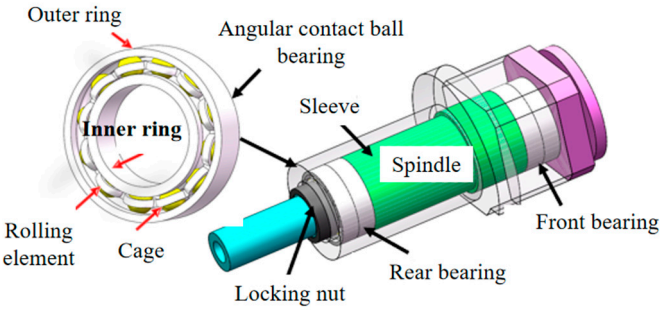
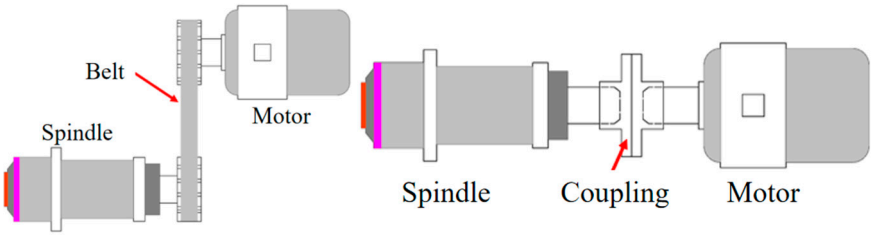


Figure 1. Spindle composition structure.



(**a**) Belt connection (**b**) Direct motor connection

Figure 2. Spindle connection types.

The following sections will study the vibration characteristics of a spindle system using the above connection types and with the bearing under thermal load, using FEM calculations. The dynamic response of the spindle rotor system is usually calculated using two common methods: the transfer matrix method and FEM. This study adopted FEM. FEM is a more complex program and requires more computing resources than the transfer matrix method. However, FEM has greater calculation accuracy and fewer elements for division than the transfer matrix method. The most important thing is to avoid the possible numerical instability seen in the transfer matrix method.

The support bearings of the spindle unit can be simplified into the form shown in Figure 3, with support stiffness in the X and Y directions of K_{xx} and K_{yy}, when analyzing the vibration characteristics of the spindle unit using FEM. The actual spindle rotor system is an elastic system with continuous mass distribution and infinite degrees of freedom. As shown in Figure 4, the system was divided into 10 Timoshenko beam elements along the axis, based on their size characteristics, to perform dynamic analysis using FEM. The rolling bearing can be simplified as a spring-damper model, with each element connected at the nodes. Analyzing the first-order natural frequency of the spindle-bearing rotor system under changing bearing support stiffness conditions has universal significance compared to calculating its specific natural frequency under known bearing support stiffness conditions because the actual bearing support stiffness varies with load and operating conditions, changing the bending vibration frequency of the spindle-bearing rotor unit along with the changes in bearing support stiffness.

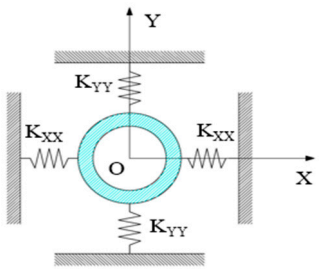


Figure 3. Equivalent model of the bearing.

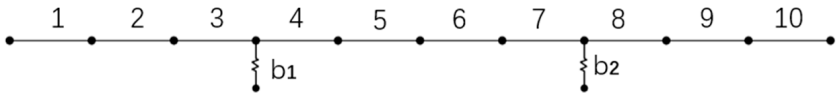


Figure 4. Finite element model of the belt-connection spindle.

When FEM was used to analyze the vibration characteristics of the spindle rotor, displacement $u\ (x, y, z)$ inside the rotor element could be expressed as a linear product of the x, y, and z coordinates and the shape function, as follows:

$$\mathbf{u}(x,y,z,t) = \mathbf{N}(x,y,z)\mathbf{q}(t) \tag{1}$$

Equation (1) can usually be written as follows:

$$\begin{Bmatrix} u_x(x,y,z,t) \\ u_y(x,y,z,t) \\ u_z(x,y,z,t) \end{Bmatrix} = \begin{bmatrix} \mathbf{N}(x,y,z) & \mathbf{0} & \mathbf{0} \\ \mathbf{0} & \mathbf{N}(x,y,z) & \mathbf{0} \\ \mathbf{0} & \mathbf{0} & \mathbf{N}(x,y,z) \end{bmatrix} \begin{Bmatrix} \mathbf{q}_x(t) \\ \mathbf{q}_y(t) \\ \mathbf{q}_z(t) \end{Bmatrix} \tag{2}$$

2.2. Simplification of the Spindle Rotation Unit

The spindle rotor in this study can be simplified as a beam element because the axial scale of the spindle rotor was much larger than the radial physical scale, and the rotor primarily had bending moments. The beam element can be divided into parts, such as the Euler–Bernoulli beam, Timoshenko beam, Vlasov beam, universal beam (GB), and high-order beam, divided according to the degrees of freedom and number of nodes. The deformation of a beam depends on many factors, like its topological form, structural dimensions, cross-sectional shape, material properties, and load boundary conditions. Reasonable assumptions and necessary simplifications must be made about the deformation mode of the beam structure when analyzing its deformation. Generally, the mechanical equilibrium equation lists partial differential equations based on the material's constitutive model. The applied mathematical analysis introduces boundary conditions and loads, followed by the use of analytical and numerical methods to solve these partial differential equations.

As shown in Figure 5, a simplified Timoshenko beam model was used to analyze the vibration characteristics of the spindle rotation element in this study. The beam element had one node at each end, with each node having 6 degrees of freedom and a total of 12 degrees of freedom.

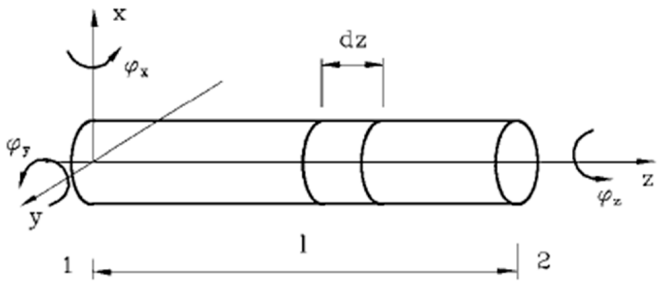


Figure 5. Beam unit.

In generalized coordinates, the displacement vector of the beam element node can be represented as follows:

$$\mathbf{q} = \left[u_{x_1}, u_{y_1}, u_{z_1}, \phi_{x_1}, \phi_{y_1}, \phi_{z_1}, u_{x_2}, u_{y_2}, u_{z_2}, \phi_{x_2}, \phi_{y_2}, \phi_{z_2}\right]^T. \tag{3}$$

According to the inherent characteristics of the beam element, vector q can be decomposed into four components, as follows:

$$\begin{array}{ll} \mathbf{q}_A = [u_{z_1}, u_{z_2}]^T, & \mathbf{q}_{F1} = [u_{x_1}, \phi_{y_1}, u_{x_2}, \phi_{y_2}]^T \\ \mathbf{q}_T = [\phi_{z_1}, \phi_{z_2}]^T, & \mathbf{q}_{F2} = [u_{y_1}, \phi_{x_1}, u_{y_2}, \phi_{x_2}]^T \end{array} \tag{4}$$

The bending vibration behavior of a beam can be represented by complex coordinate vectors, as follows:

$$\mathbf{q}_F = [u_{x_1} + iu_{y_1}, \phi_{y_1} - i\phi_{x_1}, u_{x_2} + iu_{y_2}, \phi_{y_2} - i\phi_{x_2}]^T \tag{5}$$

The shape function adopts the following form to avoid the problem of shear self-locking:

$$\begin{array}{ll} N_{11} = \frac{1+\Phi(1-\zeta)-3\zeta^2+2\zeta^3}{1+\Phi}, & N_{12} = l\zeta\frac{1+\frac{1}{2}\Phi(1-\zeta)-2\zeta+\zeta^2}{1+\Phi} \\ N_{13} = \zeta\frac{\Phi+3\zeta-2\zeta^2}{1+\Phi}, & N_{14} = l\zeta\frac{-\frac{1}{2}\Phi(1-\zeta)-\zeta+\zeta^2}{1+\Phi} \\ N_{21} = 6\zeta\frac{\zeta-1}{l(1+\Phi)}, & N_{22} = \frac{1+\Phi(1-\zeta)-4\zeta+3\zeta^2}{1+\Phi} \\ N_{23} = -6\zeta\frac{\zeta-1}{l(1+\Phi)}, & N_{24} = \frac{\Phi\zeta-2\zeta+3\zeta^2}{1+\Phi} \end{array} \tag{6}$$

where $\zeta = z/l$ is the dimensionless coordinate:

$$\Phi = \frac{12EI_y\chi}{GAl^2} \tag{7}$$

Here, χ is the shear factor and G is the gyroscopic matrix. Equation (2) can be rewritten as follows:

$$\begin{Bmatrix} u_x \\ \phi_y \end{Bmatrix} = \begin{bmatrix} N_{11} & N_{12} & N_{13} & N_{14} \\ N_{21} & N_{22} & N_{23} & N_{24} \end{bmatrix} \begin{Bmatrix} u_{x_1} \\ \phi_{y_1} \\ u_{x_2} \\ \phi_{y_2} \end{Bmatrix} \tag{8a}$$

$$\begin{Bmatrix} u_y \\ \phi_x \end{Bmatrix} = \begin{bmatrix} N_{11} & N_{12} & N_{13} & N_{14} \\ N_{21} & N_{22} & N_{23} & N_{24} \end{bmatrix} \begin{Bmatrix} u_{y_1} \\ \phi_{x_1} \\ u_{y_2} \\ \phi_{x_2} \end{Bmatrix} \tag{8b}$$

The potential energy equation of the beam element with bending and shear deformation can be represented as follows:

$$d\mathcal{U} = \frac{1}{2}EI_y\left[\left(\frac{d\phi_y}{dz}\right)^2 + \left(\frac{d\phi_x}{dz}\right)^2\right]dz + \frac{1}{2}\frac{GA}{\chi}\left(\gamma_{xz}^2 + \gamma_{yz}^2\right)dz \tag{9}$$

The relationship between shear deformation factor and displacement is as follows:

$$\gamma_{xz} = \phi_y - \frac{du_x}{dz}, \gamma_{yz} = -\phi_x - \frac{du_y}{dz} \tag{10}$$

$\mathbf{N}_1$ and $\mathbf{N}_2$ represent the first and second rows of N in Equation (8a), and $\mathbf{q}_x$ and $\mathbf{q}_y$ represent the vectors in the xz and yz planes. The entire beam element is integrated, and the potential energy equation of the beam element can be expressed as follows:

$$\begin{array}{l} \mathcal{U} = \frac{EI_y}{2l}\int_0^1 \mathbf{q}_x^T\frac{d}{dz}\mathbf{N}_2^T\frac{d}{dz}\mathbf{N}_2\mathbf{q}_x d\zeta + \frac{EI_y}{2l}\int_0^1 \mathbf{q}_y^T\frac{d}{dz}\mathbf{N}_2^T\frac{d}{dz}\mathbf{N}_2\mathbf{q}_y d\zeta \\ + \frac{6EI_y}{\Phi l}\int_0^1 \mathbf{q}_x^T\mathbf{N}_3^T\mathbf{N}_3\mathbf{q}_x d\zeta + \frac{6EI_y}{\Phi l}\int_0^1 \mathbf{q}_y^T\mathbf{N}_3^T\mathbf{N}_3\mathbf{q}_y d\zeta \end{array} \tag{11}$$

where:

$$\mathbf{N}_3 = \mathbf{N}_2 - \frac{d}{dz}\mathbf{N}_1 \tag{12}$$

After introducing the stiffness matrix, Equation (11) can be abbreviated as follows:

$$\mathcal{U} = \frac{1}{2}\mathbf{q}_x^T\mathbf{K}\mathbf{q}_x + \frac{1}{2}\mathbf{q}_y^T\mathbf{K}\mathbf{q}_y \tag{13}$$

The bending stiffness matrix $\mathbf{K}$ of the beam element is expressed as follows:

$$\mathbf{K} = \frac{EI_y}{l^3(1+\Phi)}\begin{bmatrix} 12 & 6l & -12 & 6l \\ & (4+\Phi)l^2 & -6l & (2-\Phi)l^2 \\ & & 12 & -6l \\ & \text{symm.} & & (4+\Phi)l^2 \end{bmatrix} \tag{14}$$

The dynamic equation of the beam element can be expressed as follows:

$$d\mathcal{T} = \frac{1}{2}\rho A\left(\dot{u}_x^2 + \dot{u}_y^2\right) + \frac{1}{2}\rho\left[I_y\left(\dot{\phi}_x^2 + \dot{\phi}_y^2\right) + J_p\left(\Omega^2 + 2\Omega\dot{\phi}_x\phi_y\right)\right] \tag{15}$$

Furthermore, $J_p = 2J_y$, due to the axial symmetry of the beam element on the cross-section. After introducing the shape function matrix, Equation (15) can be expressed as follows [28]:

$$\begin{array}{c} d\mathcal{T} = \frac{1}{2}\rho A\left(\dot{\mathbf{q}}_x^T\mathbf{N}_1^T\mathbf{N}_1\dot{\mathbf{q}}_x + \dot{\mathbf{q}}_y^T\mathbf{N}_1^T\mathbf{N}_1\dot{\mathbf{q}}_y\right)dz + \frac{1}{2}\rho I_y\left(\dot{\mathbf{q}}_x^T\mathbf{N}_2^T\mathbf{N}_2\dot{\mathbf{q}}_x + \right. \\ \left. + \dot{\mathbf{q}}_y^T\mathbf{N}_2^T\mathbf{N}_2\dot{\mathbf{q}}_y\right) + \rho J_y\left(\Omega^2 - 2\Omega\dot{\mathbf{q}}_y^T\mathbf{N}_2^T\mathbf{N}_2\mathbf{q}_x\right)dz \end{array} \tag{16}$$

After integrating the beam element, the dynamic energy equation of the element thus obtained is as follows:

$$\begin{array}{c} \mathcal{T} = \frac{1}{2}\rho Al\int_0^1\left(\dot{\mathbf{q}}_x^T\mathbf{N}_1^T\mathbf{N}_1\dot{\mathbf{q}}_x + \dot{\mathbf{q}}_y^T\mathbf{N}_1^T\mathbf{N}_1\dot{\mathbf{q}}_y\right)dz + \frac{1}{2}\rho I_y l\int_0^1\left(\dot{\mathbf{q}}_x^T\mathbf{N}_2^T\mathbf{N}_2\dot{\mathbf{q}}_x + \right. \\ \left. + \dot{\mathbf{q}}_y^T\mathbf{N}_2^T\mathbf{N}_2\dot{\mathbf{q}}_y\right) + \rho J_y l\Omega^2 - 2\rho J_y l\Omega\int_0^1\mathbf{q}_y^T\mathbf{N}_2^T\mathbf{N}_2\mathbf{q}_x dz \end{array} \tag{17}$$

The dynamic energy equation of a beam element can be written as follows:

$$\mathcal{T} = \frac{1}{2}\dot{\mathbf{q}}_x^T\mathbf{M}_T\dot{\mathbf{q}}_x + \frac{1}{2}\dot{\mathbf{q}}_y^T\mathbf{M}_T\dot{\mathbf{q}}_y + \frac{1}{2}\dot{\mathbf{q}}_x^T\mathbf{M}_R\dot{\mathbf{q}}_x + \frac{1}{2}\dot{\mathbf{q}}_y^T\mathbf{M}_R\dot{\mathbf{q}}_y + \rho J_y l\Omega^2 - 2\Omega\dot{\mathbf{q}}_y^T\mathbf{M}_R\mathbf{q}_x \tag{18}$$

where $\mathbf{M}_T$ and $\mathbf{M}_R$ represent the translation and rotation components in the mass matrix, respectively.

$$\mathbf{M}_T = \frac{\rho Al}{420(1+\Phi)^2}\begin{bmatrix} m_1 & lm_2 & m_3 & -lm_4 \\ & l^2m_5 & lm_4 & -l^2m_6 \\ & & m_1 & -lm_2 \\ & \text{symm.} & & l^2m_5 \end{bmatrix} \tag{19}$$

$$\mathbf{M}_R = \frac{\rho I_y}{30l(1+\Phi)^2}\begin{bmatrix} m_7 & lm_8 & -m_7 & lm_8 \\ & l^2m_9 & -lm_8 & -l^2m_{10} \\ & & m_7 & -lm_8 \\ & \text{symm.} & & l^2m_9 \end{bmatrix} \tag{20}$$

Here,

$$\begin{array}{ll} m_1 = 156 + 294\Phi + 140\Phi^2, & m_2 = 22 + 38.5\Phi + 17.5\Phi^2 \\ m_3 = 54 + 126\Phi + 70\Phi^2, & m_4 = 13 + 31.5\Phi + 17.5\Phi^2 \\ m_5 = 4 + 7\Phi + 3.5\Phi^2, & m_6 = 3 + 7\Phi + 3.5\Phi^2 \\ m_7 = 36, & m_8 = 3 - 15\Phi \\ m_9 = 4 + 5\Phi + 10\Phi^2, & m_{10} = 1 + 5\Phi - 5\Phi^2 \end{array} \tag{21}$$

And

$$\mathbf{M} = \mathbf{M}_T + \mathbf{M}_R\mathbf{G} = 2\mathbf{M}_R \tag{22}$$

Here, **M** and **G** represent the mass matrix and gyromatrix, respectively.

2.3. Simplification of the Bearing Units

The spring elements in the complex coordinate system can be represented as follows:

$$\mathbf{q} = \left[u_{x_1} + iu_{y_1}, \phi_{y_1} - i\phi_{x_1}, u_{x_2} + iu_{y_2}, \phi_{y_2} - i\phi_{x_2}\right]^T \tag{23}$$

The corresponding stiffness matrix is as found in Ref [28]:

$$\mathbf{K} = \begin{bmatrix} k & 0 & -k & 0 \\ 0 & \kappa & 0 & -\kappa \\ -k & 0 & k & 0 \\ 0 & -\kappa & 0 & \kappa \end{bmatrix} \tag{24}$$

where k and κ are the stiffness values for displacements and rotations, respectively.

3. Analysis of the Low-Order Critical Speed of the Spindle

Based on the theoretical methods introduced in the previous section, this section describes the developed corresponding calculation programs using MATLAB software (R2024b) and analyses of the vibration systems of spindle rotors with different connection forms. The material of the spindle is 25Cr2Mo1VA (density: 7.85 g/cm^3, modulusof elasticity, E: 210 GPa, and Poisson's ratio: 0.3).

3.1. Kinetic Equation

The critical speed of the spindle rotor system is usually calculated and solved on the basis of its undamped free vibration equation set. The undamped vibration characteristics of the spindle-bearing rotor system without damping can be represented as follows:

$$\left(-\Omega^2(\mathbf{M} - \mathbf{G} - \mathbf{K}_\Omega) + \mathbf{K}\right)\mathbf{q}_0 = \mathbf{0} \tag{25}$$

Here, **M** and **G** represent the mass matrix and gyromatrix, respectively. Therefore, the critical speed calculation can be transformed into an eigenvalue problem, represented as follows:

$$\det\left(-\Omega^2(\mathbf{M} - \mathbf{G} - \mathbf{K}_\Omega) + \mathbf{K}\right) = 0 \tag{26}$$

3.2. Low-Order Natural Frequency

In the structure of an electric spindle rotor system, the motor rotor of the electric spindle is directly installed on the spindle rotor. It has a larger radial size and better stiffness than a mechanical spindle with the same specifications. Consequently, the probability of resonance within the power frequency range is lower. Moreover, this study has investigated only the low-order natural frequency characteristics of the two spindle units that are more prone to resonance, to avoid repetitive work. As shown in Table 1, this research used the Timoshenko beam element as the analysis model. Additionally, it used FEM to analyze the characteristics of the first six natural frequencies of the finite element model of the spindle rotor, shown in Figure 4, as a function of bearing support stiffness.

The first four vibration frequencies of the spindle rotor system were much smaller than the power frequency of the rotor when the support stiffness of the spindle-bearing unit was in the 1×10^{-3} to 1×10^{3} N/m range. The fifth natural frequency of the spindle-bearing rotor unit was still much smaller than the power frequency of the rotor system when the bearing support stiffness was in the 1×10^{-3} to 1×10^{-1} N/m range. However, the higher-order (sixth or higher) natural frequencies of the rotor system were much larger than the power frequency of the bearing rotor system.

Table 1. Corresponding relationships between the first six vibration frequencies of the spindle rotor system and the variations in bearing support stiffness.

N/m		1×10^{-3}	1×10^{-2}	1×10^{-1}	1×10^{0}	1×10^{1}	1×10^{2}
Frequency (Hz)	1st	0	0	0	0.01	0.06	0.53
	2nd	0	0	0	0.14	0.43	1.37
	3rd	0	0.01	0.04	0.14	0.43	1.37
	4th	0	0.01	0.04	3.07	3.13	3.6
	5th	3.07	3.07	3.07	1435.01	1435.01	1435.01
	6th	1435.01	1435.01	1435.01	1447.23	1447.24	1447.24
N/m		1×10^{3}	1×10^{4}	1×10^{5}	1×10^{6}	1×10^{7}	1×10^{8}
Frequency (Hz)	1st	3.11	12.34	41.68	133.65	420.37	1136.23
	2nd	4.33	13.65	42.91	134.85	421.77	1140.34
	3rd	4.35	13.8	44.06	140.52	442.9	1275.21
	4th	6.19	15.56	45.9	142.38	444.5	1276.45
	5th	1435.01	1435.02	1435.12	1436.14	1447.22	1709.33
	6th	1447.24	1447.25	1447.35	1448.38	1459.64	1720.99
N/m		1×10^{9}	1×10^{10}	1×10^{11}	1×10^{12}	1×10^{13}	1×10^{14}
Frequency (Hz)	1st	1314.32	1323.43	1324.28	1324.37	1324.35	1324.27
	2nd	1323.06	1332.49	1333.37	1333.46	1333.44	1333.37
	3rd	2329.34	2552.57	2575.15	2577.41	2577.7	2577.84
	4th	2339.19	2565.82	2588.78	2591.08	2591.37	2591.51
	5th	4128.06	5566.39	5674.65	5684.73	5685.7	5685.9
	6th	4143.42	5602.29	5711.43	5721.57	5722.55	5722.76

As the bearing support stiffness increased, the power and natural frequencies of the bearing rotor system overlapped when the support stiffness was in the 1×10^4 to 1×10^6 N/m range. A spindle in this support stiffness range may experience resonance, affecting its cutting performance. The first-order vibration frequency of the spindle-bearing system was much higher than the working frequency of the spindle rotor system when the stiffness of the spindle-bearing support exceeded 1×10^7 N/m. Consequently, the spindle rotor system did not experience resonance within the working speed range in this case.

As shown in Figure 6, the preload force was 290 N (under normal pre-tightening conditions) and the radial support stiffness of the bearing was 3.5×10^8 N/m when the bearing was in the moderate preload range given for the 7008C angular contact ball bearing produced by the NSK company. Consequently, the first- and second-order natural frequencies of the spindle-bearing rotor system were 1120 Hz, the third- and fourth-order natural frequencies were 1523 Hz, and the fifth and sixth-order natural frequencies were 2388 Hz, according to the vibration characteristics of the spindle rotor system, these being much higher than the power frequency within the operating speed of the spindle. However, the first two vibration frequencies of the bearing rotor system entered the power frequency range when the bearing support stiffness was below 0.4×10^8 N/m, indicating poor bearing preload, which needs to be taken seriously. In particular, the spindle axial temperature distribution was uneven and had different degrees of thermal deformation in the initial stage of workpiece processing due to the thermal load effect of the previous working period. It returned to the ambient temperature after being shut down. The preload screw expands in the hot state due to the thermal expansion effect; the preload force increases and may loosen up in the cold state, leading to insufficient bearing preload in the initial stage of the screw's next use. At that point, the first two natural frequencies of the bearings corresponding to the spindle-bearing rotor system may be within the power frequency range. If the spindle is raised to working speed within a short period of time, it may cause resonance in the spindle system and lead to unnecessary economic losses. Additionally, the outer surface of the spindle bearing's outer ring and the bearing chamber were in a gap-fit state at the beginning. Moreover, the bearing had low radial stiffness. Without preheating treatment, resonance may occur in the spindle when the spindle speed increases to the

working speed within a short period of time. However, this resonance has a short duration. In this experiment, the outer ring expanded, and the contact stiffness between the outer ring and the spindle-bearing chamber increased with the increased bearing heat, thereby increasing the radial support stiffness of the bearing. Consequently, the bending vibration frequency was much higher than the power frequency. For this reason, keeping the spindle in an idle state at a lower speed for a period when starting a machine tool is necessary, followed by increasing it to the working speed for cutting after the system stabilizes.

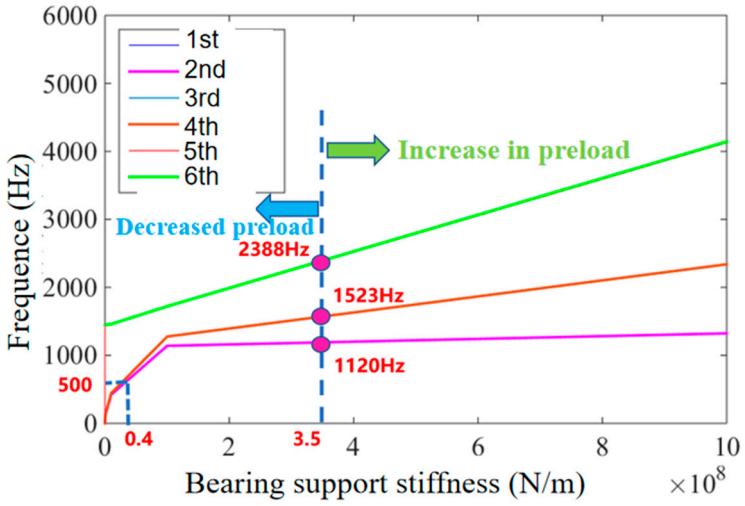


Figure 6. Vibration characteristics of the spindle rotor system.

3.3. Analysis of the Vibration Characteristics of a Direct-Coupled Spindle Rotor

An analysis of the variation law of the support stiffness of the bearing unit under thermal load and the variation of the vibration characteristics of the separated spindle system with bearing support stiffness showed that the separated spindle system may resonate within the power frequency range in some special cases. The vibration characteristics of the direct connection system of the motor spindle differed, due to the different connection forms compared to the separated spindle system.

The bearing rotor system of the direct coupled motor spindle system shown in Figure 2b was simplified to study its vibration characteristics, and the Timoshenko beam element was used for finite element division. A finite element analysis model of the direct coupled motor spindle rotor system of a certain type of machining center is shown in Figure 7. This model consists of 18 beam elements, connected to each other at the nodes. K1 and K2 represent the constraints at the front and rear bearings of the spindle element. K3 and K4 represent the constraints at the motor rotor bearings. For this study, it was assumed that the spindle element bearings had the same support stiffness as the motor rotor support to simplify the analysis process, where K1 = K2 = K3 = K4.

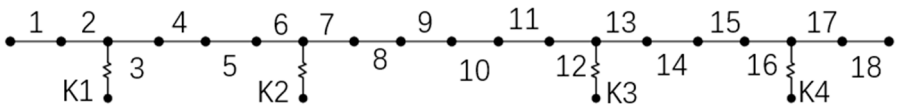


Figure 7. Finite element model of the direct spindle rotation unit.

The specific values of the variations in the first six natural vibration frequencies of the motor spindle direct-coupled rotor system, along with the stiffness of the support bearing, are shown in Table 2. Like the separated spindle system, the first four natural vibration frequencies of the direct spindle system approached zero when the support stiffness of the spindle bearing was in the 1×10^{-3} to 1×10^{1} N/m range. The natural vibration frequency of the direct spindle system gradually increased with the increased support stiffness of the

bearing. The first three natural vibration frequencies of the direct spindle system were in the power frequency range when the support stiffness of the bearing was in the 1×10^4 to 1×10^6 N/m range, causing probable resonance in the direct spindle system. Moreover, the first six natural vibration frequencies of the direct spindle system would be much higher than the power frequency of the spindle unit for a further increase in the bearing support stiffness (exceeding 1×10^7 N/m).

Table 2. Corresponding relationship between the first six order vibration frequencies of the directly connected spindle rotor system and the variations in bearing support stiffness.

N/m		$\mathbf{1 \times 10^{-3}}$	$\mathbf{1 \times 10^{-2}}$	$\mathbf{1 \times 10^{-1}}$	$\mathbf{1 \times 10^{0}}$	$\mathbf{1 \times 10^{1}}$	$\mathbf{1 \times 10^{2}}$
Frequency (Hz)	**1st**	0	0	0	0.01	0.1	0.68
	2nd	0	0	0	0.11	0.35	1.08
	3rd	0.01	0.01	0.04	0.11	0.36	1.18
	4th	0.01	0.01	0.04	1.63	1.73	2.4
	5th	1.62	1.62	1.62	353.11	353.11	353.11
	6th	353.11	353.11	353.11	362.88	362.88	362.89
N/m		$\mathbf{1 \times 10^{3}}$	$\mathbf{1 \times 10^{4}}$	$\mathbf{1 \times 10^{5}}$	$\mathbf{1 \times 10^{6}}$	$\mathbf{1 \times 10^{7}}$	$\mathbf{1 \times 10^{8}}$
Frequency (Hz)	**1st**	2.89	9.75	31.29	99.31	312.47	942.86
	2nd	3.29	10.13	31.67	99.68	312.74	942.97
	3rd	4.09	13.88	45.1	143.43	442.13	1271.72
	4th	5.32	15.12	46.35	144.77	444.62	1275.46
	5th	353.14	353.41	356.09	381.97	584.07	1386.64
	6th	362.91	363.18	366.85	391.64	592.66	1395.44
N/m		$\mathbf{1 \times 10^{9}}$	$\mathbf{1 \times 10^{10}}$	$\mathbf{1 \times 10^{11}}$	$\mathbf{1 \times 10^{12}}$	$\mathbf{1 \times 10^{13}}$	$\mathbf{1 \times 10^{14}}$
Frequency (Hz)	**1st**	2018.66	2083.14	2088.78	2089.34	2089.42	2089.65
	2nd	2028.33	2093.71	2099.44	2100	2100.06	2100.33
	3rd	2265.52	2797.65	2843.46	2847.9	2848.33	2846.86
	4th	2266.93	2803.56	2849.97	2854.47	2854.91	2855.90
	5th	2716.12	3359.73	3465.11	3475.99	3477.07	3478.30
	6th	2720.78	3366.06	3472.08	3483.03	3484.12	3485.87

According to the physical structure of the directly connected spindle system, it had a more prominent axial size than the separated spindle system, and it had smaller higher-order natural vibration frequencies than the separated spindle system. Similarly, the first three natural frequencies of the separated and the directly connected spindle systems underwent significant changes when the bearing support stiffness was 1×10^5, 1×10^6, 1×10^7, 1×10^8, and 1×10^9 N/m, indicating that the vibration frequency of the spindle rotor system was sensitive to the bearing support stiffness in this range, and attention must be paid to controlling the change in the bearing support stiffness to avoid falling into the resonance range. This was because the internal heat source of the machine tool began to heat up after it was turned on, increasing the temperature at various positions. The machine tool underwent thermal deformation, constantly approaching a specific stable state over time, which is usually dynamically stable with changes in environmental temperature. Generally, the machining accuracy is unstable during the first period of functioning after turning the machine tool on, due to the unstable thermal deformation of various components. Therefore, waiting for the bed temperature to be relatively stable is recommended before proceeding with the actual machining process.

As shown in Figure 8, the first six natural frequencies of the direct-coupled spindle rotor system had an upward trend with increased bearing support stiffness. Similar to the separated spindle system, the first two vibration frequencies of the direct-coupled spindle rotor system were 1081 Hz, the third and fourth vibration frequencies were 1500 Hz, and the fifth and sixth vibration frequencies were 1682 Hz for the bearings in a normal pre-tightening state, this being much higher than the power frequency needed for the spindle unit to not cause system resonance. However, it cannot be ruled out that the spindle system

may experience resonance within this power frequency range in some special cases. The widely used axial positioning pre-tightening method is simpler to complete and can reduce spindle manufacturing costs since most spindle bearings are fixed using this method rather than axial fixed-pressure preloading. However, the locking nut used for axial positioning pre-tightening loosens up with the progression of working time, decreasing the preload of the bearing unit. Additionally, the outer surface of the bearing's outer ring and the bearing chamber continue to wear down during use, further increasing the reserved installation gap. Both these situations may decrease the radial and axial support stiffness of the spindle rotor unit. The first two vibration frequencies of the direct spindle system enter the power frequency range when the radial support stiffness is less than 0.5×10^8 N/m. The system may have resonance when the spindle drives the tool for cutting, affecting the cutting accuracy of the machine tool. The axial vibration frequency of the rotor unit is usually tens of times the bending vibration frequency, this being much higher than its power frequency. Therefore, this study does not discuss the impact of the axial vibration characteristics of the spindle rotor system on the machining performance of the machine tool.

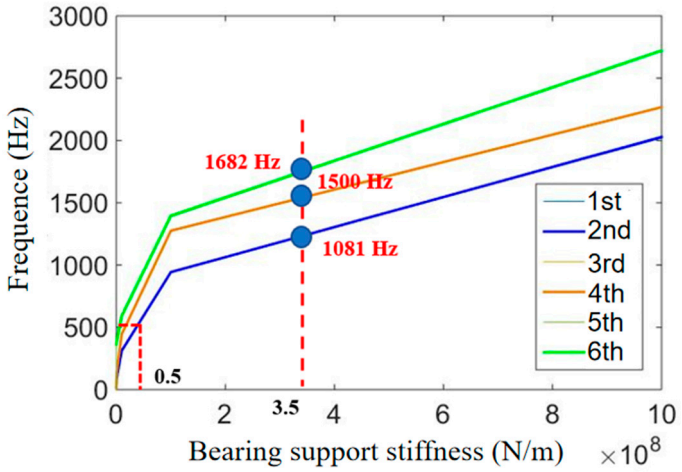


Figure 8. Vibration frequency variation characteristics of the direct spindle rotor system.

In summary, the power frequency in the working speed of the spindle was much lower than the first-order natural frequency of the bearing rotor system under a normal preload, regardless of the connection method of the spindle, so this did not cause resonance in the spindle. Usually, the significant vibration of the spindle in industrial sites is due to the dynamic balance failure of the spindle unit rather than to resonance. Therefore, the dynamic balance of the spindle should be measured using a dynamic balance instrument to check for any dynamic balance failure in the spindle unit when the vibration amplitude of the spindle unit exceeds the maximum allowable value for processing. This study analyzed the vibration characteristics of the spindle under two common connection methods and the effect of the bearing support stiffness of the spindle system on the vibration frequency of the system. Additionally, it indirectly discussed the impact of increased heat generation in the bearing on the vibration frequency of the spindle system with the increased spindle speed. Furthermore, a free-mode experiment using the spindle rotor system was designed to determine if the natural frequency of the spindle rotor system conformed to the finite element analysis results and if resonance would occur in the power frequency range under normal preloading, to study the vibration characteristics of the spindle unit.

4. Experiment

To demonstrate the reliability of the FEM results, this section discusses the use of experimental methods to validate the simulation results.

4.1. Experiment Design

For this task, a free-mode experiment using the spindle system was designed, and the LMS test platform was used to measure the low-order natural frequencies and free vibration modes of the spindle rotor and assembly, in order to verify the reliability of the finite element thermal dynamic simulation analysis of the spindle rotor system and understand the vibration characteristics of the spindle system. The experimental scheme is shown in Figure 9. A few measuring points were set in the axial direction of the tested object (spindle rotor and assembly), and a hammer was used to sequentially strike the rotor in the horizontal direction of each measuring point to generate vibrations. Simultaneously, the vibration response of the spindle in the horizontal direction was measured, and the signal was transmitted to the LMS testing and analysis system through a three-phase acceleration sensor to evaluate the natural frequencies of each order of the system. During the measurement, seven and five acceleration sensors were installed on the spindle assembly and the rotor, respectively.

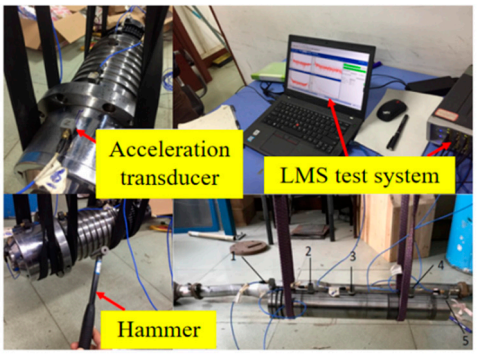


Figure 9. Spindle free mode experiment setup.

Notably, secondary contact between the force hammer and the striking object needs to be avoided after percussion when using a force hammer for percussion experiments; otherwise, the accuracy of the measurement results will be affected. The distribution diagram of the low-order natural frequencies of the tested spindle rotor is shown in Figure 10. The first four natural frequencies were 1373.4, 3342.8, 5515, and 8459.7 Hz. The first two bending modes of the rotor are shown in Figure 11. According to Table 1, during normal preloading, the first-order free vibration frequency of the spindle in finite element analysis is 1198.3 Hz. The experimental result was 1376 Hz, with a certain difference and an error of 12.9%. This was mainly caused by factors such as grid division, model simplification, and uneven materials, which are inevitable. Therefore, the results of the finite element analysis in this study are acceptable. The measurement results indicated that the rotor had a much higher vibration frequency than the working frequency. The separated spindle rotor, when operating within the power frequency range, would not cause resonance in the spindle system, eliminating the need to consider its impact on the machining accuracy of the machine tool. However, in this instance, the belt used for hanging the spindle in the experiment and the ideal elastic belt were different. The actual belt that was used was not completely elastic, thereby introducing corresponding constraints to the spindle. Consequently, the measured vibration frequency of the spindle was higher than the actual value. Therefore, the actual power frequency of the spindle rotor was lower than its test frequency.

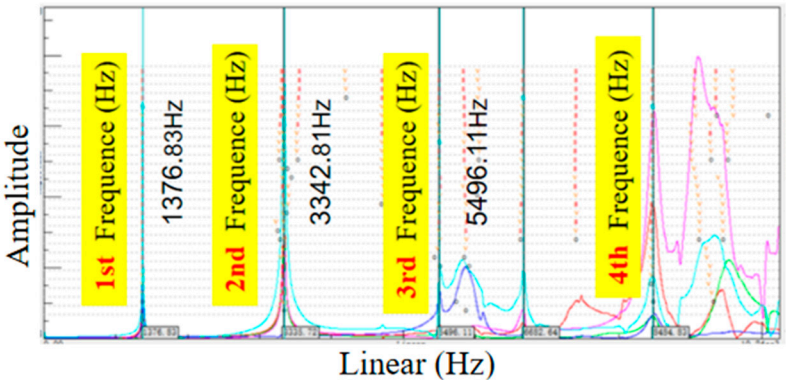
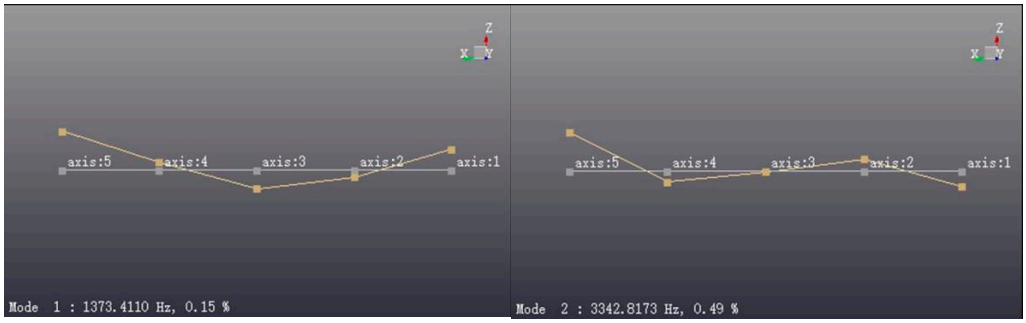


Figure 10. Low-order frequency distribution of the spindle rotor.



(**a**) (**b**)

Figure 11. Spindle rotor vibration mode: (**a**) first-order vibration mode; (**b**) second-order vibration mode.

4.2. Analysis of the Experimental Results

The low-order natural frequency distribution test results for the spindle assembly are shown in Figure 12. According to the measured results, the first- and second-order natural frequencies were 831.4 and 1581.9 Hz, respectively. The third-order natural frequency inferred from the measured results was 2365.58 Hz since the force hammer did not excite a significant third-order mode in the spindle. The first two orders of vibration modes of the spindle assembly are shown in Figure 13. The lateral constraint load that was introduced was much greater than the elastic band used in the experiment because the spindle casing was fixed to the machine tool using a locking nut during spindle installation. Therefore, the vibration frequency of the spindle assembly under actual constraints exceeded the experimentally measured value.

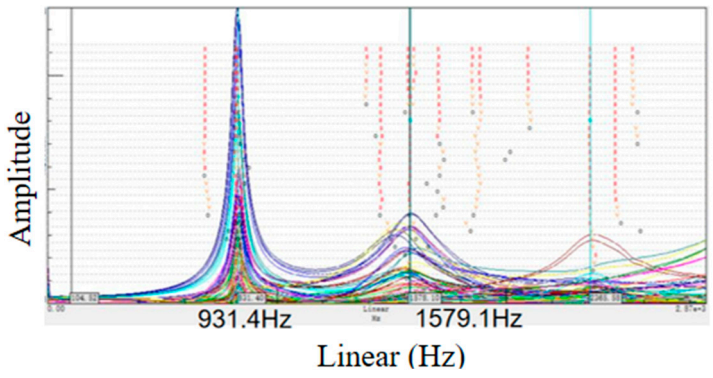
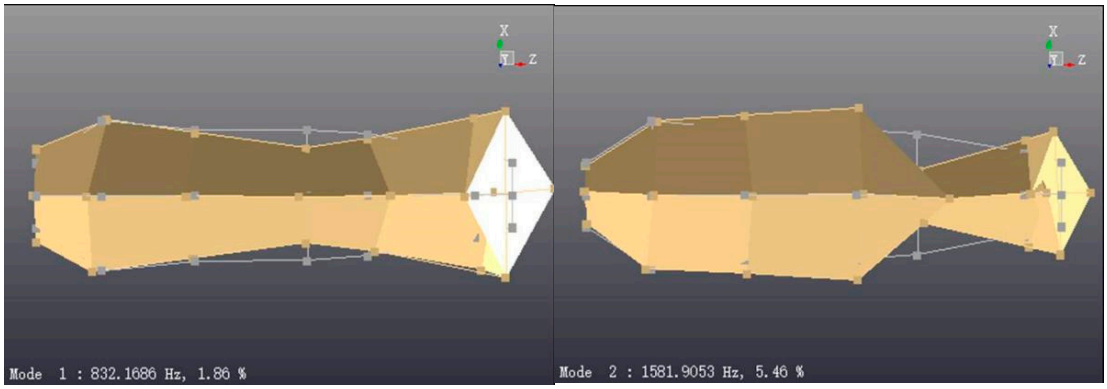


Figure 12. Low-order frequency distribution of the spindle assembly.



(**a**) (**b**)

Figure 13. Vibration-mode diagram of the spindle assembly: (**a**) first order; (**b**) second order.

The free vibration frequency of the spindle assembly was lower than the vibration frequency of the spindle rotor. Consequently, this result seemed to violate the relevant mechanical vibration theory. The spindle rotor appeared to be more slender than the spindle assembly, and its first-order natural frequency was more easily excited. However, the actual measured results were not the same. Instead, the first-order vibration frequency of the assembly appeared at a lower frequency. Additionally, it reflected the complexity of the vibration law of the spindle system, which cannot be judged based on experience. This study concluded that the lower-order natural frequencies of the spindle assembly and rotor were outside their power frequency range. Therefore, the resonance of the spindle under normal preloading would not appear at that power frequency.

Furthermore, this study showed the feasibility of using finite element analysis to analyze the dynamic characteristics of spindle units. This method can be used to analyze the vibration frequency of the spindle units, based on the radial support stiffness of the spindle bearings. Additionally, it could determine whether the spindle would stimulate its own resonance within the power frequency range based on the usage of spindle units, in order to take measures to improve spindle stiffness. However, accurately determining the vibration frequency of a spindle under specific conditions is challenging for various reasons. First, the finite element model was simplified based on solid features, and the finite element analysis model omitted some spindle solid features compared to the actual model. Second, the spindle rotor was connected to the bearing and was subjected to radial constraints from the bearing in the finite element simulation, but it was in a completely free state under experimental conditions. Additionally, the measuring instruments had certain analytical errors. Often, in practical engineering applications, only determining the low-order natural frequency range of the spindle rotor unit to determine the vibration situation of the rotor system is necessary.

This study analyzed the impact of temperature rise on the structural vibration characteristics of a spindle during normal use. Moreover, other factors often affect the spindle during use, resulting in unstable dynamic performance. Frequently, the cutting materials contaminate spindle-bearing grease when workpieces are processed with powdered chips, due to the harsh environments. Additionally, the authors found that the majority of spindles repaired at a spindle factory were damaged due to spindle-bearing grease contamination and dynamic balance failure, resulting in spindle-bearing burns. All bearings are replaced when repairing a spindle, even if only one pair of bearings has been burned, since dismantling the damaged bearings also damages the structures of other unburned bearings and causes serious waste. This deteriorates the lubrication characteristics of the spindle, decreasing its thermal dynamic characteristics and service life. Additionally, this study did not analyze the influence of the changes in the physical state of the bearing assembly on bearing stiffness. The influence of bearing components on bearing stiffness can be referred to in other, recent studies [29–37]. Krsti et al. used artificial neural networks (ANNs)

to predict friction torque and temperature in axial angular contact ball bearings, which provided a predictive model that improves our understanding of bearing performance under different operational conditions [29]. Xu et al. investigated how surface friction and varying lubricant oil temperatures impact the time-varying stiffness of roller bearings. The authors developed a model to assess thermal effects on stiffness characteristics, highlighting how temperature variations caused by friction can influence bearing performance, which provided important insights for optimizing roller bearing design and improving operational reliability under different thermal conditions [36].

Furthermore, exploring the key factors affecting the vibration characteristics of a spindle unit is a significant research direction for the authors of this study in the future. In future research, we plan to continue studying the variation characteristics of spindle vibration when the spindle's stiffness changes (axial preload force changes). In addition, our team is also preparing to conduct fatigue life tests on the spindle, studying the changes in spindle lifespan caused by changes in preload force under no-load conditions. In the future, our team will continue to study the factors affecting the service life of the spindle under cutting conditions and will conduct comprehensive analyses to summarize which are the main factors and which are the secondary factors.

5. Conclusions

The abnormal vibration of spindles has always been a key concern for researchers. Based on the Timoshenko beam model and rotor dynamic theory, this study used FEM analysis to analyze the vibration characteristics of the spindle rotor system and obtained some valuable research results:

(1) The authors thoroughly analyzed the influence of the spindle bearing heat on the stiffness of the spindle system and obtained the resonance conditions of the spindle rotor within the power frequency range.
(2) The general law of the variation of the low-order vibration frequency of the spindle-bearing system with the stiffness of the supporting bearing was determined.
(3) It was concluded that the low-order natural frequencies of the spindle assembly and rotor were outside their power frequency range.
(4) Additionally, the resonance of the spindle would not manifest at a power frequency under normal preloading.

In fact, the health status of the spindle is closely related to its vibration frequency and speed. Research has found that when the vibration frequency of the spindle operates at a speed of 12,000 r/min, if its vibration frequency is lower than 200 Hz, it will be affected by abnormal vibrations during startup, which will subsequently weaken the health status of the spindle and reduce its service life. Similarly, when the working speed of the spindle is 30,000 r/min, if its vibration frequency is lower than 50 Hz, abnormal vibration will occur during startup and operation, thereby reducing its service life. The specific service life of the spindle is also affected by other factors, such as cutting depth, usage time, and dynamic imbalance. Therefore, accurately predicting the service life of the spindle is not an easy task. However, we can extend the service life of the spindle by avoiding those factors that may affect its lifespan as much as possible. This study proposes a new method for diagnosing spindle faults, which can help researchers better understand the operating status of a spindle. However, the findings have some inevitable shortcomings, due to the conditions and level of this study. The authors intend to continue to improve the level of the study in future works.

Author Contributions: Conceptualization, L.Z. and Z.W.; methodology, Z.W.; software, L.Z.; validation, L.Z. and Z.W.; formal analysis, L.Z.; investigation, L.Z.; resources, Z.W.; data curation, Z.W.; writing—original draft preparation, L.Z. and Z.W.; writing—review and editing, L.Z.; visualization, L.Z. and Z.W.; supervision, L.Z. and Z.W.; project administration, L.Z. and Z.W.; funding acquisition, L.Z. and Z.W. All authors have read and agreed to the published version of the manuscript.

Funding: This research was funded by the National Natural Science Foundation of China (grant nos. 62241205), Zunyi Technology and Big Data Bureau, Moutai Institute Joint Science and Technology Research and Development Project (grant nos. ZSKHHZ [2022] No.170, No.171), Moutai High level talent project (grant nos. mygccrc [2022]109, mygccrc [2022]111, KY [2020]223).

Data Availability Statement: The data presented in this study are available on request from the corresponding author due to the nature of this research.

Acknowledgments: The authors appreciate the financial support from the National Natural Science Foundation of China (grant nos. 62241205), Zunyi Technology and Big Data Bureau, Moutai Institute Joint Science and Technology Research and Development Project (grant nos. ZSKHHZ [2022] No.170, No.171), Moutai High level talent project (grant nos. mygccrc [2022]109, mygccrc [2022]111, KY [2020]223).

Conflicts of Interest: The authors declare no conflicts of interest.

References

1. Cui, Z.P.; Zhang, H.J.; Zong, W.J.; Li, G.; Du, K. Origin of the lateral return error in a five-axis ultraprecision machine tool and its influence on ball-end milling surface roughness. *Int. J. Mach. Tools Manuf.* **2022**, *178*, 103907. [CrossRef]
2. Sepahi-Boroujeni, S.; Mayer, J.R.R.; Khameneifar, F.; Woźniak, A. A full-covariance uncertainty assessment in on-machine probing. *Int. J. Mach. Tools Manuf.* **2021**, *167*, 103768. [CrossRef]
3. Ibaraki, S.; Okumura, R. A machining test to evaluate thermal influence on the kinematics of a five-axis machine tool. *Int. J. Mach. Tools Manuf.* **2021**, *163*, 103702. [CrossRef]
4. Huang, C.R.; Lu, M.C. Investigation of Cutting Path Effect on Spindle Vibration and AE Signal Features for Tool Wear Monitoring in Micro Milling. *Appl. Sci.* **2023**, *13*, 1107. [CrossRef]
5. Diez-Olivan, A.; Del Ser, J.; Galar, D.; Sierra, B. Data fusion and machine learning for industrial prognosis: Trends and perspectives towards Industry 4.0. *Inf. Fusion* **2019**, *50*, 92–111. [CrossRef]
6. Danylchenko, Y.; Storchak, M.; Danylchenko, M.; Petryshyn, A. Cutting Process Consideration in Dynamic Models of Machine Tool Spindle Units. *Machines* **2023**, *11*, 582. [CrossRef]
7. Zhan, W.; Siyang, C.; Zhongxian, Z.X. Research for the bearing fit effect on the vibration characteristics of spindle rotor-bearing system. *J. Mech. Sci. Technol.* **2023**, *37*, 6257–6270.
8. Chen, D.; Zhang, X.; Sun, K.; Fan, J. Analysis and optimization of main influencing factors on vibration offset of aerostatic spindle. *Ind. Lubr. Tribol.* **2022**, *74*, 498–506. [CrossRef]
9. Wang, Z.; Zhang, K.; Wang, Z.; Bai, X.; Wang, Q. Research on vibration of ceramic motorized spindle influenced by interference and thermal displacement. *J. Mech. Sci. Technol.* **2021**, *35*, 2325–2335. [CrossRef]
10. Hao, J.; Li, C.; Song, W.; Yao, Z.; Miao, H.; Xu, M.; Gong, X.; Lu, H.; Liu, Z. Thermal-mechanical dynamic interaction in high-speed motorized spindle considering nonlinear vibration. *Int. J. Mech. Sci.* **2023**, *240*, 107959. [CrossRef]
11. Alfares, M.; Saleem, O.; Majeed, M. Analytical study of thermal variation impact on dynamics of a spindle bearing system. *Proc. Inst. Mech. Eng. Part K J. Multi-Body Dyn.* **2019**, *233*, 871–898. [CrossRef]
12. Liu, H.; Zhang, Y.; Li, C.; Li, Z. Nonlinear dynamic analysis of CNC lathe spindle-bearing system considering thermal effect. *Nonlinear Dyn.* **2021**, *105*, 131–166. [CrossRef]
13. Zhang, Y.; Wang, L.; Zhang, Y.; Zhang, Y. Design and thermal characteristic analysis of motorized spindle cooling system. *Adv. Mech. Eng.* **2021**, *13*, 168781402110208. [CrossRef]
14. Dong, Y.; Chen, F.; Lu, T.; Qiu, M. Research on thermal stiffness of machine tool spindle bearing under different initial preload and speed based on FBG sensors. *Int. J. Adv. Manuf. Technol.* **2022**, *119*, 941–951. [CrossRef]
15. Truong, D.S.; Kim, B.-S.; Ro, S.-K. An analysis of a thermally affected high-speed spindle with angular contact ball bearings. *Tribol. Int.* **2021**, *157*, 106881. [CrossRef]
16. Liu, J.; Li, F.; Yong, J.; Lai, T.; Zhang, P. Investigation of spindle-tool assembly dynamics for optical grinding motorized spindles. *Optik* **2020**, *216*, 164836. [CrossRef]
17. Cao, Z.; Kang, H.; Liu, H.; Duan, L.; Ouyang, Z.; Zhou, Y.; Jiang, G.; Li, W. Modeling and dynamic response of variable mass system of maglev turning electric spindle. *Nonlinear Dyn.* **2023**, *111*, 255–274. [CrossRef]
18. Shi, J.; Cao, H.; Maroju, N.K.; Jin, X. Dynamic Modeling of Aerostatic Spindle With Shaft Tilt Deformation. *J. Manuf. Sci. Eng.* **2020**, *142*, 021006. [CrossRef]
19. Ye, W.; Guo, Y.; Liang, R.; Xu, J. Research on Thermo-Mechanical Coupling Deformation for the Ball Screw of Machine Tool Spindle Feed System. *J. Vib. Eng. Technol.* **2020**, *8*, 443–454. [CrossRef]
20. Cao, W.; Li, H.; Li, Q. A method of thermal error prediction modeling for CNC machine tool spindle system based on linear correlation. *Int. J. Adv. Manuf. Technol.* **2022**, *118*, 3079–3090. [CrossRef]
21. Fu, G.; Zhou, L.; Zheng, Y.; Lu, C.; Wang, X.; Xie, L. Improved unscented Kalman filter algorithm-based rapid identification of thermal errors of machine tool spindle for shortening thermal equilibrium time. *Measurement* **2022**, *195*, 111121. [CrossRef]

22. Lu, Q.; Zhu, D.; Wang, M.; Li, M. Digital Twin-Driven Thermal Error Prediction for CNC Machine Tool Spindle. *Lubricants* **2023**, *11*, 219. [CrossRef]
23. Miao, H.; Wang, C.; Hao, J.; Li, C.; Xu, M.; Liu, Z. Dynamic analysis of the column-spindle system considering the nonlinear characteristics of kinematic joints. *Mech. Mach. Theory* **2022**, *174*, 104922. [CrossRef]
24. Xu, H.; Ma, H.; Wen, B.; Yang, Y.; Li, X.; Luo, Z.; Han, Q.; Wen, B. Dynamic characteristics of spindle-bearing with tilted pedestal and clearance fit. *Int. J. Mech. Sci.* **2023**, *261*, 108683. [CrossRef]
25. Tian, J.; Wang, P.; Xu, H.; Ma, H.; Zhao, X. Nonlinear vibration characteristics of rolling bearing considering flexible cage fracture. *Int. J. Non-Linear Mech.* **2023**, *156*, 104478. [CrossRef]
26. Hou, S.; Lin, R.; Hou, L.; Chen, Y. Dynamic characteristics of a dual-rotor system with parallel non-concentricity caused by inter-shaft bearing positioning deviation. *Mech. Mach. Theory* **2023**, *184*, 105262. [CrossRef]
27. Liu, J.; Xue, L.; Xu, Z.; Wu, H.; Pan, G. Vibration characteristics of a high-speed flexible angular contact ball bearing with the manufacturing error. *Mech. Mach. Theory* **2021**, *162*, 104335. [CrossRef]
28. Genta, G. *Dynamics of Rotating Systems*; Springer US: New York, NY, USA, 2005.
29. Krstić, V.; Milčić, D.; Madić, M.; Milčić, M.; Milovančević, M. Prediction of Friction Torque and Temperature on Axial Angular Contact Ball Bearings for Threaded Spindle Using Artificial Neural Network. *J. Vib. Eng. Technol.* **2022**, *10*, 1473–1480. [CrossRef]
30. Du, X.; Wu, L.; Miao, J.; Li, X.; Chen, B. Time-varying contact characteristics of the planetary roller screw mechanism considering nonuniform surface waviness. *Tribol. Int.* **2023**, *187*, 108668. [CrossRef]
31. Deng, S.; Zhao, C.; Yang, C.; Qian, D.; Jiang, S. Correlation between vibration and power consumption of angular contact ball bearings under structural size combinations based on nonlinear dynamic model. *Nonlinear Dyn.* **2023**, *111*, 16021–16047. [CrossRef]
32. Wu, X.; Qin, Y.; Luo, J.; Wang, S.; Chen, B. Fault dynamic model of high-speed rolling bearing by a compound displacement excitation function considering the effect of defect roughness. *Mech. Mach. Theory* **2022**, *177*, 105061. [CrossRef]
33. Wen, C.; Meng, X.; Fang, C.; Gu, J.; Xiao, L.; Jiang, S. Dynamic behaviors of angular contact ball bearing with a localized surface defect considering the influence of cage and oil lubrication. *Mech. Mach. Theory* **2021**, *162*, 104352. [CrossRef]
34. Xie, Y.H.; Xu, L.X.; Deng, Y.Q. A dynamic approach for evaluating the moment rigidity and rotation precision of a bearing-planetary frame rotor system used in RV reducer. *Mech. Mach. Theory* **2022**, *173*, 104851. [CrossRef]
35. Zhang, C.; Wei, J.; Wang, F.; Hou, S.; Zhang, A.; Lim, T.C. Dynamic model and load sharing performance of planetary gear system with journal bearing. *Mech. Mach. Theory* **2020**, *151*, 103898. [CrossRef]
36. Hao, X.; Zhai, J.; Liang, J.; Chen, Y.; Han, Q. Time-varying stiffness characteristics of roller bearing influenced by thermal behavior due to surface frictions and different lubricant oil temperatures. *Tribol. Int.* **2020**, *144*, 106125. [CrossRef]
37. Fang, B.; Cheng, M.; Gu, T.; Ye, D. An improved thermal performance modeling for high-speed spindle of machine tool based on thermal contact resistance analysis. *Int. J. Adv. Manuf. Technol.* **2022**, *120*, 5259–5268. [CrossRef]

Disclaimer/Publisher's Note: The statements, opinions and data contained in all publications are solely those of the individual author(s) and contributor(s) and not of MDPI and/or the editor(s). MDPI and/or the editor(s) disclaim responsibility for any injury to people or property resulting from any ideas, methods, instructions or products referred to in the content.